



In-Situ Hydrothermal Growth of Bi-Hierarchical ZnO Nanoarchitecture with Surface Modification for Efficient Hybrid Solar Cells



Yan-Zhen Zheng^{a,b}, Haiyang Ding^c, Yu Liu^a, Xia Tao^{a,*}, Guozhong Cao^d, Jian-Feng Chen^b

^a State Key Laboratory of Organic-Inorganic Composites, Beijing University of Chemical Technology, Beijing 100029, China

^b Research Center of the Ministry of Education for High Gravity Engineering & Technology, Beijing University of Chemical Technology, Beijing 100029, China

^c General Research Institute for Nonferrous Metals, Beijing 100088, China

^d Department of Materials Science and Engineering, University of WA, Seattle, WA 98195, USA

ARTICLE INFO

Article history:

Received 20 April 2014

Received in revised form 24 June 2014

Accepted 13 August 2014

Available online 3 September 2014

Keywords:

organic-inorganic hybrid solar cells
dye
surface modification
hierarchical zinc oxide nanoarchitecture
one-dimension

ABSTRACT

The ability to fabricate hierarchical one-dimensional (1D) ZnO nanoarchitecture with a high degree of multifunctionalities by suitable synthetic strategies still represents a vital issue towards boosting the ultimate photoelectric conversion efficiency of organic-inorganic hybrid solar cells (HSCs). We herein synthesize a hierarchical 1D ZnO nanoarchitecture i.e. ZnO NAR/NR grown on a dual-dimension seeded layer via an all-solution chemical bath deposition process. It is found that ZnO NAR/NR nanoarchitecture can accelerate electron separation and the D205 dye uptake, and hence simultaneously maximizing the key features of photoelectrode in HSCs i.e. carrier generation and charge transport. A remarkable efficiency of 1.30% is achieved under 1 sun illumination for D205-modified hierarchical ZnO HSC fabricated with a very thin layer of ZnO NAR/NR (thickness $\sim 1 \mu\text{m}$) and a significant improvement is evaluated with respect to a reference photoanode made from ZnO nanorods.

© 2014 Elsevier Ltd. All rights reserved.

1. Introduction

Organic-inorganic hybrid solar cells (HSCs) based on heterojunctions of conjugated polymers and n-type metal oxide nanocrystals have attracted great interest owing to the ease of processibility from solution and potential for making low-cost and up-scalable solar cells with the good chemical and physical stability [1–5]. Similar to the bulk heterojunction organic solar cells, insufficient connection between metal oxide nanocrystals causes the carrier-transport limitation in the hybrid photovoltaic cells by the poorly formed electron conducting pathway in the polymer-oxide nanocrystal interface [6]. It has been demonstrated that the charge-transport property can be improved by blending oriented ZnO nanorods (ZnO NR) with polymers because the single-crystalline ZnO NR can provide a near trap-free transporting path through hopping and a better physical connectivity with polymer [7–12]. A promising hybrid photovoltaic device consisting of oriented ZnO NR and conjugated polymer has been exploited, in which ZnO NR with high electron mobility provide a direct and ordered electron conducting path for photogenerated electrons to

the collecting electrode [7–10,12–14]. Such HSCs based on pure ZnO NR and poly(3-hexylthiophene) (P3HT) have attained photo-to-electron conversion efficiencies from initial 0.07% climbing to 0.76% [8,10], still less than that of ZnO nanocrystal/P3HT based cell [5]. The disappointing power conversion efficiency (η) of oriented ZnO NR/P3HT based solar cells might be ascribed to insufficient contact area between the oriented ZnO NR and carrier generation polymer P3HT. It remains a challenge to achieve sufficient-surface-area with good contact and efficient charge transfer from polymer to oxide [15,16]. An efficient solution to the enhance HSC efficiency is to develop a large-surface-area framework i.e., ZnO nanosheet (ZnO NS) from 1D ZnO array. An efficiency of 0.88% was achieved by ZnO NS-P3HT HSC [16].

Another approach to boost light harvesting and carrier generation and transfer within ZnO HSC is to modify the surface chemistry of the inorganic materials, aiming to improve the chemical compatibility between polymer and ZnO NR array [15,17–19]. The ZnO surface modification with a thin layer of organic molecules was found to improve the interfacial energetic and surface-wetting properties, leading to enhanced cell performance. For example, notable efficiencies of 0.71% and 1.16% were achieved in the HSC based on ZnO NR-P3HT and ZnO NS-P3HT functionalized with a metal-free organic dye D205 and D149, respectively [19,20]. Notwithstanding, few efficiencies based on

* Corresponding author. Tel.: +86 10 6445 3680; fax: +86 10 6443 4784.

E-mail address: taoxia@yahoo.com (X. Tao).

ZnO NR-P3HT HSCs could exceed the above-mentioned value because of the incomplete polymer infiltration governed by ZnO NR array morphology and the insufficient interface area between ZnO NR array and P3HT polymer.

Hierarchical structure composed of various building blocks on the nanoscale can combine several opposite peculiarities into one donor/acceptor electrode film, and thus endow the active electrode layer with better photoelectrochemical performance superior to single-structured electrode materials [21–24]. In this respect, design and development of suitable synthetic strategies is crucial to provide the electrode film with the desired property control. Related to ZnO, the solution-based chemical bath deposition (CBD) synthesis has been extensively used because of its convenient manufacture together with flexible control over the size and morphology of ZnO nanoarchitecture. In the present work, we report an innovative hierarchical one-dimensional ZnO nanoarchitecture i.e. ZnO NAR/NR on a dual-dimension seeded layer consisting of ZnO NR grown on ZnO nanocrystals (ZnO NC) and derived ZnO nanorods (ZnO NAR) grown on ZnO nanocrystalline aggregates (ZnO NA) via a CBD process, and the implementation of D205 modified ZnO NAR/NR as photoelectrode for use in high-efficiency HSCs (see the microstructure of the HSC in Scheme 1a). This fascinating hierarchical ZnO nanoarchitecture could simultaneously accelerate electron separation and D205 uptake, and hence simultaneously maximizing the key features of photoelectrode material in HSC, which are generally incompatible with one another: substantial light harvesting, and favorable charge generation and transport. As a result, a remarkable efficiency of 1.30% is achieved for D205 modified ZnO NAR/NR-P3HT HSC, which is 32.7% higher than that of D205 modified ZnO NR-P3HT HSC ($\eta = 0.98\%$), and far larger than that of unmodified ZnO NR-P3HT cell ($\eta = 0.22\%$).

2. Experimental

2.1. Materials

Zinc acetate dihydrate ($(\text{CH}_3\text{COO})_2\text{Zn}$), Zinc nitrate hexahydrate ($\text{Zn}(\text{NO}_3)_2 \cdot 6\text{H}_2\text{O}$), hexamethylenetetramine ($(\text{CH}_2)_6\text{N}_4$), monoethanolamine, 2-methoxyethanol, Poly(3-hexylthiophene) (P3HT), 1,2-dichlorobenzene and chenodeoxycholic acid were purchased from Sigma. Acetone, acetonitrile, diethylene glycol ($(\text{HOCH}_2\text{CH}_2)_2\text{O}$), tert-butyl alcohol and anhydrous ethanol (analytical grade purity) were obtained from Beijing Chemical Works and were used without further purification. Indoline dye D205 was

obtained from Shanghai Green Technology Co. Ltd. All solutions used in this work were prepared with $18.2 \text{ M}\Omega \text{ cm}^{-1}$ water produced by a reagent water system (Easy pure II, Barnstead).

2.2. Preparation of ZnO NAR/NR

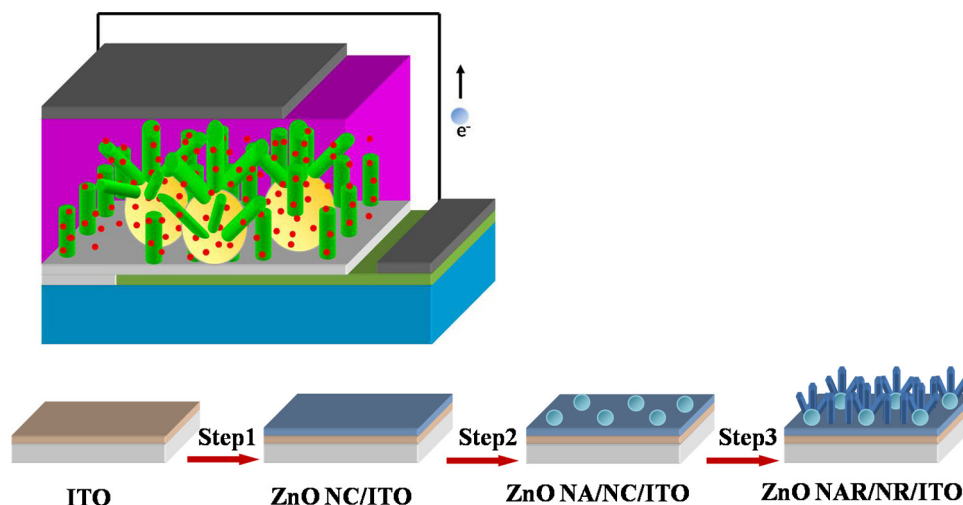
For constructing ZnO NAR/NR film, a key innovative idea lies in utilizing a complex seed layer consisting of nanometer-sized ZnO NC and submicrometer-sized ZnO NA. ZnO NAR/NR films were prepared via a simple CBD method, as illustrated in Scheme 1b. In brief, dense ZnO NC seeded layer was deposited on ITO substrates by spin-coating using zinc acetate solution (0.75 M) with a mixture of monoethanolamine in 2-methoxyethanol, then the films were annealed at 300°C for 20 min. ZnO NA was synthesized by the solvothermal process of zinc salt in polyol medium at 160°C . For preparing ZnO NA/NC hybrid seeded layer, ZnO NA was formed onto ZnO NC seeded layer by means of spin-coating method following by sintered at 350°C for 60 min. The CBD of ZnO NAR/NR photoanodes was performed by suspending the as-prepared ZnO NA/NC-seeded substrate in a 100 mL Teflon-lined stainless steel autoclave filled with 60 mL of aqueous growth solution of $\text{Zn}(\text{NO}_3)_2 \cdot 6\text{H}_2\text{O}$ and $(\text{CH}_2)_6\text{N}_4$ (25 mM). The reaction was conducted at 91.5°C for 1.5 h. The substrates were carefully rinsed with distilled water several times and finally annealed at 150°C for 30 min. For comparison, ZnO NR films were also fabricated under identical condition except various CBD times for 1.0, 1.25, 1.5, 1.75 and 2.0 h.

2.3. Surface modification by D205 molecules

The as prepared ZnO NR and ZnO NAR/NR substrates were immersed in 0.5 mM D205 (Aubonne, Switzerland) and 1.0 mM chenodeoxycholic acid in acetonitrile/tert-butyl alcohol (V/V = 1:1) for approximately 50 min at 60°C . Then the substrates were rinsed thoroughly by acetonitrile before cell fabrication.

2.4. Fabrication of hybrid ZnO-P3HT solar cells

P3HT solution (10 mg mL^{-1} , dissolved in 1,2-dichlorobenzene) was then spin-coated onto the (dye-modified) ZnO NAR/NR or ZnO NR films (900 rpm for 9 s, followed by 2500 rpm for 50 s), and then heated at 125°C for 5 min to facilitate the filtration of P3HT into ZnO nanoarchitecture. The films were then transferred into the high vacuum chamber ($3 \times 10^{-4} \text{ Pa}$). Ag top electrode was subsequently evaporated onto the P3HT layer in the vacuum



Scheme 1. (a) Schematic structure of ZnO NAR/NR-based HSC. (b) Schematic diagram illustrating the process for the formation of ZnO NAR/NR film.

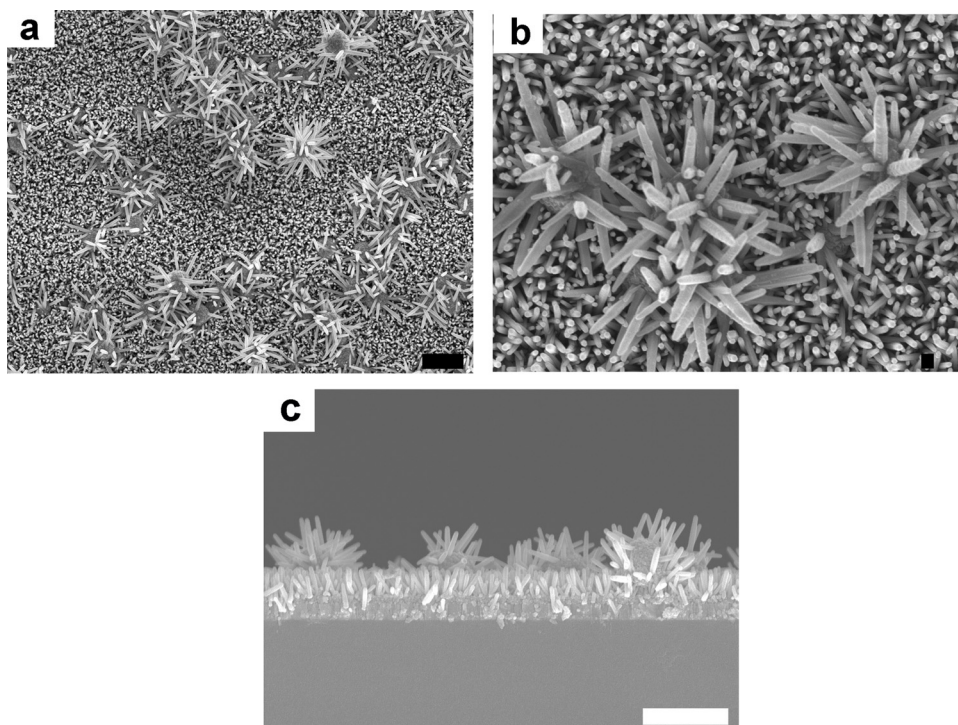


Fig. 1. Plan-view (a&b) and cross-sectional (c) SEM images of ZnO NAR/NR film. Scale bars are $1\ \mu\text{m}$ for images a&c and $100\ \text{nm}$ for image b, respectively.

evaporation system. The active area of the resulting cell exposed in light was approximately $0.10\ \text{cm}^2$.

2.5. Characterization

The morphologies and microstructures of ZnO NAR/NR films were examined using a JEOL JSM-6701 F field emission scanning electron microscope. The light absorption properties of the samples were investigated by UV-visible light absorption/diffused reflectance spectrometry (Lambda 950, Perkin Elmer). Photovoltaic measurements were carried out under simulated AM 1.5 sunlight illumination with $100\ \text{mW cm}^{-2}$ light output. A $1000\ \text{W}$ xenon lamp (Thermo Oriel, America) served as the light source. Current-Voltage characterization of hybrid cells was performed using electrochemical station (CHI660C, ShangHai). Monochromatic light in the range of $400 - 800\ \text{nm}$ was obtained by using a series of filters and the incident photo to current conversion efficiency (IPCE) measurement was performed on a Keithley Model 2000 Source Meter. Time-resolved photoluminescence (TRPL) spectroscopy measurements were performed using a pulse laser ($365\ \text{nm}$) with a pulse width of $100\ \text{ps}$ for excitation. The TRPL decays at $650\ \text{nm}$ were recorded using a time correlated single photon counting spectrometer.

3. Results and Discussion

Fig. 1 a&b exhibit SEM images of ZnO NAR/NR film where dotted ZnO NA and dense ZnO NC are simultaneously served as seeds for nanorods growth. Vertical ZnO NR grown on ITO substrate are $\sim 400\ \text{nm}$ in length, and omni-directional nanorods grown on $500 \sim 700\ \text{nm}$ -sized aggregates are $200 \sim 600\ \text{nm}$ in length (**Fig. 1** c). The ZnO NR and ZnO NAR number densities are controlled to be $\sim 1.8 \times 10^{10}\ \text{cm}^{-2}$ and $6.5 \times 10^4\ \text{cm}^{-2}$, respectively (**Fig. 1** a). For comparison, oriented ZnO NR on ITO substrate, as shown in **Fig. 2** a&b, is also fabricated via CBD method under identical experimental condition. The average length of oriented ZnO NR is $\sim 450\ \text{nm}$. A large difference between ZnO NAR/NR and

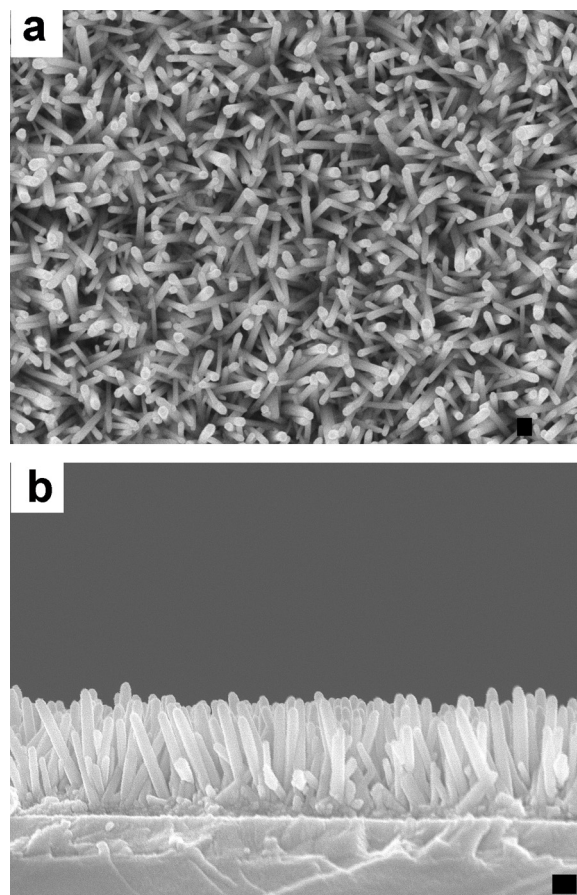


Fig. 2. Plan-view (a) and cross-sectional (b) SEM images of ZnO NR film growing for $1.5\ \text{h}$. Scale bar: $100\ \text{nm}$.

ZnO NR lies in the varying orientation of nanorods. Additionally, SEM images of ZnO NR growing with various periods are also provided in Fig. S1. We can see that the nanorod length augments when prolonging CBD growth periods (also see Table S1). In order to clearly examine P3HT infiltration ability within the ZnO NAR/NR framework, we are motivated to prepare a thin ZnO NAR/NR-P3HT hybrid by spin-coating an extra thin P3HT layer onto ZnO NAR/NR film. From top-view SEM image of the ZnO NAR/NR-P3HT film (Fig. 3a), P3HT coating looks not smooth owing to difference height between ZnO NR and ZnO NAR. P3HT with uniform thickness coats (~ 100 nm) onto the ZnO NAR/NR films, as shown in Fig. 3b. Heterogeneous interface and voided space can also be seen in P3HT-ZnO NAR/NR film. The adsorption amount of D205 dye on the two nanoarchitectures is estimated using UV-vis absorption spectra. It shows a dye uptake of 5.93×10^{-9} mol cm $^{-2}$ for ZnO NR, and 7.38×10^{-9} mol cm $^{-2}$ for ZnO NAR/NR, respectively. The enhanced dye uptake for ZnO NAR/NR may be ascribed to the introduction of ZnO NA with relatively large surface area in fabricating ZnO NAR/NR film [20,22]. Compared with ZnO NR, dye uptake of ZnO NAR/NR shows a 24.5% increase. This enhancement is reasonable based on sparse ZnO NAR scattering into ZnO NR film. (see Fig. 1a&b) Furthermore, the reflectance spectra of ZnO NAR/NR and ZnO NR were also examined in this work (see Fig. S2). Compared to the ZnO NR film, the ZnO NAR/NR film exhibits a stronger reflectance in the region of 410–800 nm. This indicates that submicron-sized ZnO NAR, as the light-scattering centers, makes a contribution to the enhancement in light-harvesting capability of the electrode film.

The variation of absorption spectra of ZnO NAR/NR and ZnO NR before and after D205 dye modification and P3HT addition are shown in Fig. 4. Compared with the unmodified ZnO NAR/NR, a

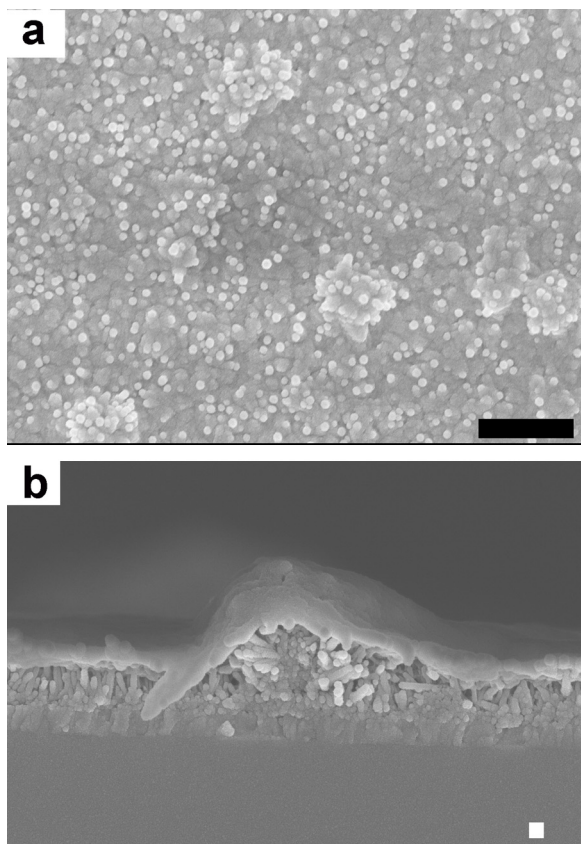


Fig. 3. Plan-view (a) and cross-sectional (b) SEM images of P3HT infiltrated ZnO NAR/NR film. Scale bars are 1 μ m for image a and 100 nm for image b, respectively.

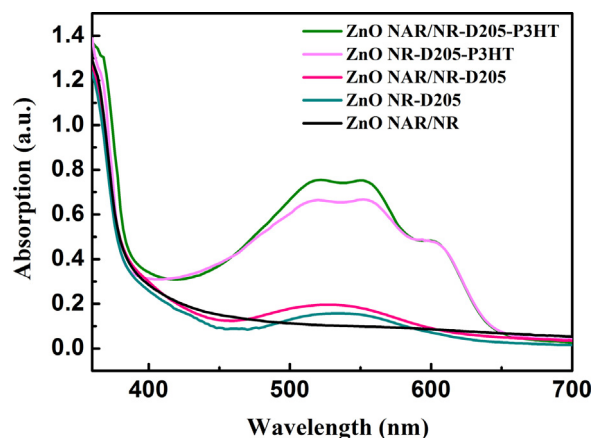


Fig. 4. UV-vis absorption spectra for ZnO NR and ZnO NAR/NR films before and after D205 dye modification as well as P3HT infiltration.

discernable light absorption enhancement in range of 470 \sim 600 nm occurring in the spectra of D205-modified ZnO NAR/NR film indicates that D205 dye molecules are adsorbed on the ZnO NAR/NR. The light absorption of D205-modified ZnO NAR/NR film is higher than that of D205-modified ZnO NR film in the range of 400 \sim 800 nm. After P3HT coating onto ZnO NAR/NR, a significant increase of light absorption from 410 nm to 650 nm is observed, indicating that P3HT has a large contribution in light absorption of ZnO films. It is worth pointing out that in comparison with P3HT, D205 also plays a role concerning light absorption of the ZnO NAR/NR film. Furthermore, in comparison to ZnO NR-D205-P3HT hybrid, the absorption spectra of ZnO NAR/NR-D205-P3HT hybrid shows slightly higher absorption in the range of 500 \sim 600 nm. As ZnO NAR/NR does not lead to a thicker P3HT coating on ZnO film surface (see Fig. 3b), the slightly higher light absorption could be ascribed to the additional absorption of sunlight contributed by more D205 adsorption and better P3HT infiltration within the ZnO NAR/NR nanoarchitectured film. Thus, it can be reasonably argued that the presence of ZnO NR within ZnO NR is favorable to P3HT penetration and D205 dye adsorption.

Fig. 5 shows the Raman spectra of P3HT pristine film (on ITO), ZnO NR-P3HT and ZnO NAR/NR-P3HT hybrids excited at 532 nm. The Raman spectra display two peaks of the in-plane ring skeleton stretch modes of the thiophene at 1445 \sim 1450 (C=C symmetric stretching) and ~ 1380 cm $^{-1}$ (C-C intraring stretching), and the

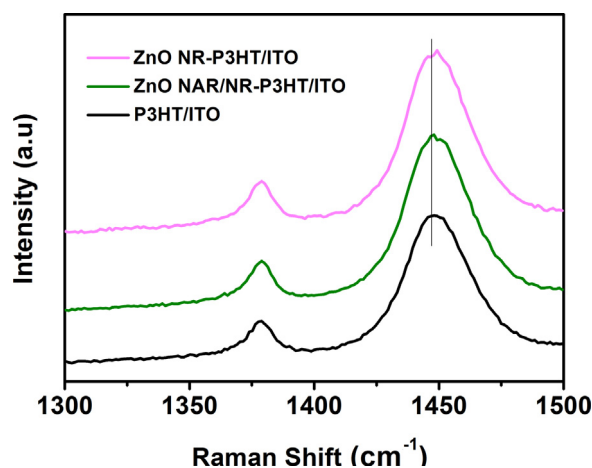


Fig. 5. Raman spectra of ZnO NR-P3HT, ZnO NR-D205-P3HT and ZnO NAR/NR-D205-P3HT hybrids.

Raman peak position of the symmetric C=C stretch mode can be used to characterize the degree of P3HT molecular order [16]. From this figure, it can be seen that the C=C stretch mode of P3HT pristine film is centered at 1447 cm^{-1} . For the ZnO NAR/NR-P3HT hybrid, the C=C mode peak position remains unaltered, indicating a better internal order within the P3HT domain. On the contrast, the C=C mode peak position that of the ZnO NR-P3HT hybrid shifts to 1449 cm^{-1} , and this means less degree of P3HT molecule ordering in the ZnO NR-P3HT hybrid [25,26]. Better internal ordering within P3HT domains is obtained when P3HT is infiltrated into the ZnO NAR/NR nanoarchitecture, which is comparable with the pristine P3HT.

To investigate the effect of nanorod length as well as D205 modification on the device performance, the photocurrent density (J)-voltage (V) characteristics of HSCs based on the D205-modified and unmodified ZnO NR-P3HT growing for different CBD time were measured under the AM 1.5 sunlight illumination (100 mW cm^{-2}). Fig. 6 shows the photovoltaic parameters of unmodified- and D205 modified- hybrid devices fabricated with a group of ZnO NR films with different length. It is obvious that D205 surface modification significantly increases short circuit current (J_{sc}), open circuit voltage (V_{oc}) and η of ZnO NR HSCs. Furthermore, for both unmodified and D205 modified ZnO NR HSCs, dye adsorption amount and J_{sc} enhance with increasing

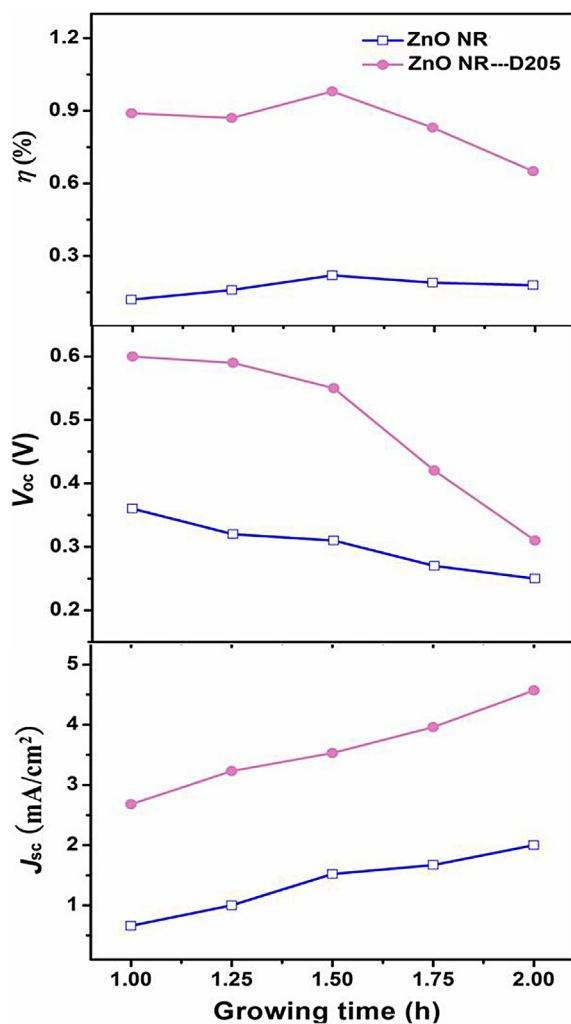


Fig. 6. Photovoltaic parameters of unmodified- and D205 modified- hybrid devices fabricated with ZnO NR films growing for different CBD times.

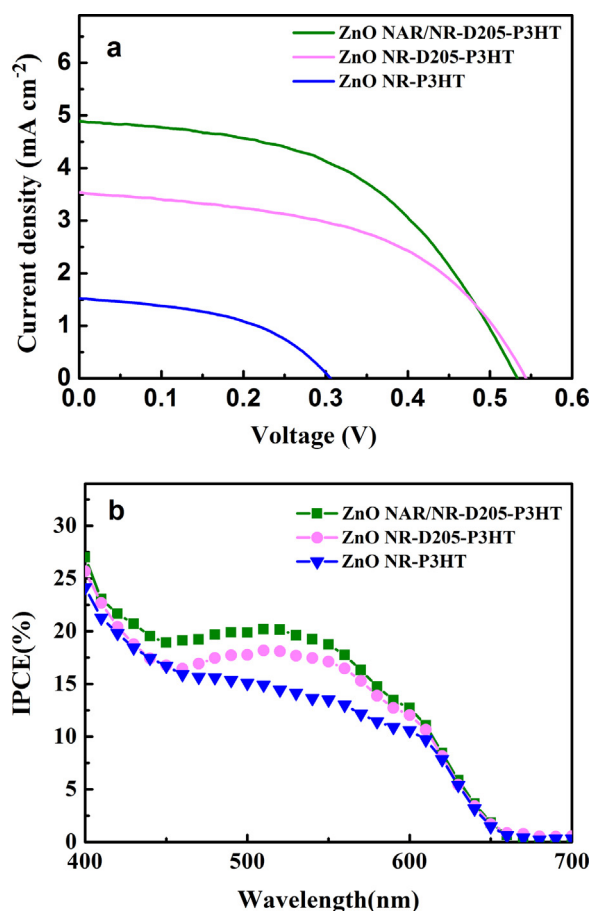


Fig. 7. (a) I - V curves and (b) IPCE plots of ZnO NR-P3HT and ZnO NR-D205-P3HT and ZnO NAR/NR-D205-P3HT HSCs.

ZnO NR length (see Table S1 and Fig. S1), but V_{oc} shows the opposite trend, leading to an optimal efficiency obtained by the film thickness of $\sim 450\text{ nm}$. It is likely that thick ZnO NR-P3HT layer requires longer electron transport time, prolonging exciton diffusion length and allows much higher possibility of the relaxation of the exciton and the recombination of the separated charges, resulting in a lower V_{oc} [27–30]. For $\sim 450\text{ nm}$ -thickness ZnO NR, the photovoltaic performance of D205 modified HSC ($J_{sc} = 3.53\text{ mA cm}^{-2}$, $V_{oc} = 0.55\text{ V}$, ff of 0.51, $\eta = 0.98\%$) is better than that of unmodified cell ($J_{sc} = 1.52\text{ mA cm}^{-2}$, $V_{oc} = 0.31\text{ V}$, $ff = 0.46$, $\eta = 0.22\%$).

To study the influence of ZnO hierarchical nanoarchitecture on the photovoltaic performance of cells, the D205 modified- HSC based on ZnO NAR/NR is also examined under the AM 1.5 sunlight illumination, as shown in Fig. 7a. The photovoltaic parameters of the three hybrid devices are summarized in Table 1. One can see that for ZnO NAR/NR-D205-P3HT HSC, J_{sc} of 4.89 mA cm^{-2} , V_{oc} of 0.53 V , and ff of 0.50 are achieved, yielding an η of 1.30%, which is improved in terms of J_{sc} and η as compared to those of ZnO

Table 1
Comparison of J_{sc} , V_{oc} , ff , and η for HSCs based on ZnO NR-P3HT, ZnO NR-D205-P3HT and ZnO NAR/NR-D205-P3HT.

Cells	J_{sc} (mA cm^{-2})	V_{oc} (V)	ff	η (%)
ZnO NR-P3HT	1.52	0.31	0.46	0.22
ZnO NR-D205-P3HT	3.53	0.55	0.51	0.98
ZnO NAR/NR-D205-P3HT	4.89	0.53	0.50	1.30

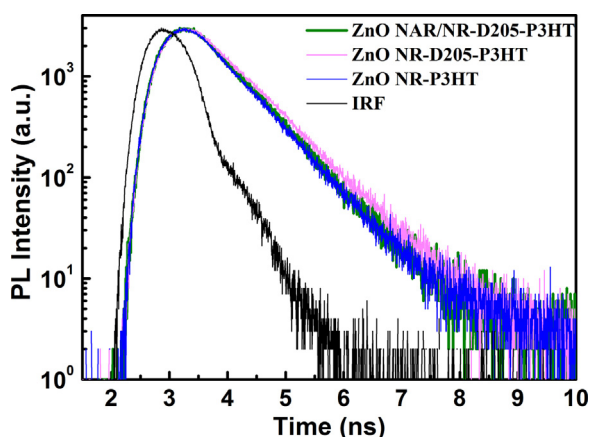


Fig. 8. TRPL decay curves of ZnO NR-P3HT, ZnO NR-D205-P3HT and ZnO NAR/NR-D205-P3HT hybrids.

NR-P3HT cell. IPCE measurement is performed for unmodified ZnO NR, dye-modified ZnO NR and ZnO NAR/NR-based HSCs and the results are shown in Fig. 7b. Obviously, for HSC with D205 modification, the IPCE values of ZnO NR hybrid cell in the range from 460 nm to 600 nm are found to be higher than that of unmodified ZnO NR hybrid cell. After adding ZnO NAR, the IPCE values of D205-modified ZnO NAR/NR-based hybrid cell further enhance in the spectrum region of 460 ~ 600 nm, which also corroborates with the higher J_{sc} of ZnO NAR/NR-D205-P3HT HSC as displayed in Fig. 7a.

The dynamics of charge separation at the interfaces between ZnO NAR/NR-P3HT or ZnO NR-P3HT in the hybrids are investigated by TRPL. Fig. 8 exhibits the TRPL decay curves of ZnO NR-P3HT, ZnO NR-D205-P3HT and ZnO NAR/NR-D205-P3HT hybrids on ITO substrates. The instrument response function (IRF) is first eliminated from the decay curves and the decay is subsequently analyzed by biexponential decay kinetics [16,31]. The average PL lifetimes of the three ZnO-P3HT hybrids are 518 ps for ZnO NR-P3HT, 606 ps for ZnO NR-D205-P3HT, and 539 ps for ZnO NAR/NR-D205-P3HT, respectively. It is evident that in comparison with ZnO NR-P3HT hybrid, the increase in PL lifetime of ZnO NR-D205-P3HT hybrid suggests that D205 retards the charge separation in ZnO NR-P3HT hybrid. This result verifies that D205 suppresses the P3HT infiltration, in consistence with the published work. [32,33] This seems to be contrary to the

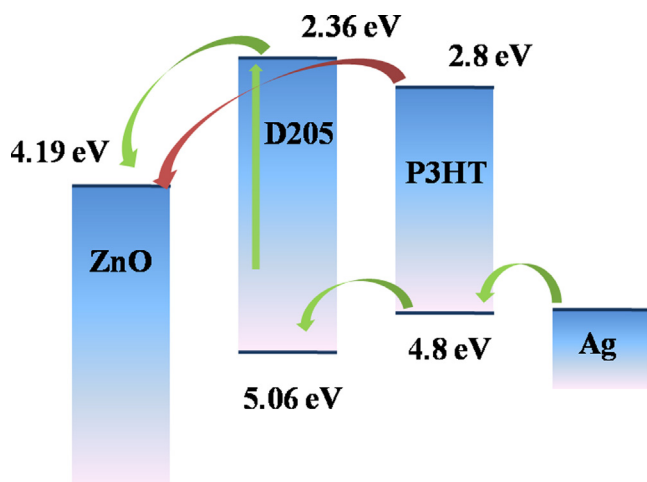


Fig. 9. Energy level diagrams and charge transfer process of hybrid device fabricated from P3HT/D205/ZnO.

photovoltaic behavior (I-V measurement). However, comparing with ZnO NR-D205-P3HT hybrid, PL lifetime of ZnO NAR/NR-D205-P3HT hybrid is reduced. This means that the presence of ZnO NAR within ZnO NR film facilitates charge separation owing to enhanced interfacial area [16], which is also evidenced by large amount dye adsorbed on the ZnO NAR/NR film.

Dye molecules to modify semiconductor oxides could have complicated impacts on zinc oxide/P3HT hybrid solar cells. D205 absorbs the incident light and contributes to the charge generation, while P3HT with a higher HOMO level than D205 acts as the hole transporter for the oxidized dye molecule regeneration [17,34]. The proposal mechanism is schemed in Fig. 9 (green arrows), and also known as the “dye-regeneration” mechanism [17]. However, D205 has a higher LUMO level than P3HT, implying an energy barrier for electron transfer from P3HT to ZnO (see the red arrow in Fig. 9) [17,35]. Thus, D205 modification disfavors charge separation in the ZnO/P3HT interface (see Fig. 8). The coating of D205 molecules on the surface of ZnO with dipole moments perpendicular to the ZnO surface, has been demonstrated to be able to widen the positive space-charge layer at the interface and subsequently induce a strong internal electric field in ZnO leading to a built-in voltage [19]. The built-in voltage would suppress the charge recombination, generating high V_{oc} . Our experimental results also verify this point (see Fig. 6). Thus, enhanced charge generation and internal electric field caused by introduction of D205 dye molecules, together with favorable charge separation and P3HT infiltration due to the presence of ZnO NAR within ZnO NR film all improved power conversion efficiency of ZnO nanoarchitected HSCs from 0.22% to 1.30%.

4. Conclusions

In summary, we report preparation of hierarchical ZnO nanoarchitecture i.e. ZnO NAR/NR on a dual-dimension seeded layer via CBD method and the implementation of D205 modified ZnO NAR/NR as photoelectrode for heterojunction hybrid solar cell. D205 surface modification enhanced optical absorption and suppressed charge recombination, though retarded charge separation in ZnO based HSCs. The hierarchical ZnO nanoarchitecture was proven to simultaneously accelerate electron separation and increase D205 uptake, and hence simultaneously maximizing the key features of both photoelectrode material and D205 in HSC, which are generally incompatible with one another: substantial carrier generation and favorable charge transport. A remarkable efficiency of 1.30% was achieved for D205-modified ZnO NAR/NR-P3HT HSC and a significant improvement was evaluated with respect to a reference photoanode made from ZnO NR. Such nanoarchitecture is expected to have similar enhancement in power conversion efficiency in dye-sensitized or quantum-dot sensitized solar cells, as well as other devices for energy conversion applications.

Acknowledgements

This work was supported financially by National Nature Science Foundation of China (NSFC) (21176019, 21121064, 21476019), Beijing Higher Education Young Elite Teacher Project (YETP0487), the Fundamental Research Funds for the Central Universities (ZZ) and 863 project (2013AA031901). YZZ would also acknowledge the scholarship from China Scholarship Council (CSC).

Appendix A. Supplementary data

Supplementary data associated with this article can be found, in the online version, at <http://dx.doi.org/10.1016/j.electacta.2014.08.077>.

References

- [1] W.U. Huynh, J.J. Dittmer, A.P. Alivisatos, Hybrid nanorod-polymer solar cells, *Science* 295 (2002) 2425–2427.
- [2] J.S. Liu, T. Tanaka, K. Sivula, A.P. Alivisatos, J.M.J. Frechet, Employing end-functional polythiophene to control the morphology of nanocrystal-polymer composites in hybrid solar cells, boosting infrared light harvesting by molecular functionalization of metal oxide/polymer interfaces in efficient hybrid solar cells, *J. Am. Chem. Soc.* 126 (2004) 6550–6551.
- [3] Y.Y. Lin, C.-W. Chen, T.-H. Chu, W.-F. Su, C.-C. Lin, C.-H. Ku, J.-J. Wu, C.-H. Chen, Nanostructured metal oxide/conjugated polymer hybrid solar cells by low temperature solution processes, *J. Mater. Chem.* 17 (2007) 4571–4576.
- [4] G. Grancini, R.S.S. Kumar, A. Abrusci, H.-L. Yip, C.-Z. Li, A.-K.Y. Jen, G. Lanzani, H. J. Snaith, Boosting infrared light harvesting by molecular functionalization of metal oxide/polymer interfaces in efficient hybrid solar cells, *Adv. Funct. Mater.* 22 (2012) 2160–2166.
- [5] S.D. Oosterhout, M.M. Wienk, S.S.V. Bavel, R. Thiedmann, L.J.A. Koster, J. Gilot, J. Loos, V. Schmidt, R.A.J. Janssen, The effect of three-dimensional morphology on the efficiency of hybrid polymer solar cells, *Nat. Mater.* 8 (2009) 818–824.
- [6] J. Weickert, R.B. Dunbar, H.C. Hesse, W. Wiedemann, L. Schmidt-Mende, Nanostructured organic and hybrid solar cells, *Adv. Mater.* 23 (2011) 1810–1828.
- [7] Y.-J. Lee, M.T. Lloyd, D.C. Olson, R.K. Grubbs, P. Lu, R.J. Davis, J.A. Voigt, J.W.P. Hsu, Optimization of ZnO nanorod array morphology for hybrid photovoltaic devices, *J. Phys. Chem. C* 113 (2009) 15778–15782.
- [8] P. Atienzar, T. Ishwara, B.N. Illy, M.P. Ryan, B.C. O'Regan, J.R. Durrant, J. Nelson, Control of photocurrent generation in polymer/ZnO nanorod solar cells by using a solution-processed TiO₂ overlayer, *J. Phys. Chem. Lett.* 1 (2010) 708–713.
- [9] D.C. Olson, Y.J. Lee, M.S. White, N. Kopidakis, S.E. Shaheen, D.S. Ginley, J.A. Voigt, J.W.P. Hsu, Effect of polymer processing on the performance of poly(3-hexylthiophene)/ZnO nanorod photovoltaic devices, *J. Phys. Chem. C* 111 (2007) 16640–16645.
- [10] L. Baeten, B. Conings, H.G. Boyen, J. D'Haen, A. Hardy, M. D'Olieslaeger, J.V. Manca, M.K. Van Bael, Towards efficient hybrid solar cells based on fully polymer infiltrated ZnO nanorod arrays, *Adv. Mater.* 23 (2011) 2802–2805.
- [11] D.K.-P. Wong, C.-H. Ku, Y.-R. Chen, G.-R. Chen, J.-J. Wu, Enhancing electron collection efficiency and effective diffusion length in dye-sensitized solar cells, *ChemPhysChem* 10 (2009) 2698–2702.
- [12] Y.-Y. Lin, T.-H. Chu, S.-S. Li, C.-H. Chuang, C.-H. Chang, W.-F. Su, C.-P. Chang, M.-W. Chu, C.-W. Chen, Interfacial nanostructuring on the performance of polymer/TiO₂ nanorod bulk heterojunction solar cells, *J. Am. Chem. Soc.* 131 (2009) 3644–3649.
- [13] A.L. Briseno, T.W. Holcombe, A.I. Boukai, E.C. Garnett, Steve W. Shelton, J.J.M. Fréchet, P. Yang, Oligo- and polythiophene/ZnO hybrid nanowire solar cells, *Nano Lett.* 10 (2010) 334–340.
- [14] Y.-Y. Lin, Y.-Y. Lee, L. Chang, J.-J. Wu, C.-W. Chen, The influence of interface modifier on the performance of nanostructured ZnO/polymer hybrid solar cells, *Appl. Phys. Lett.* 94 (2009) 63308.
- [15] J. Huang, Z. Yin, Q. Zheng, Applications of ZnO in organic and hybrid solar cells, *Energy Environ. Sci.* 4 (2011) 3861–3877.
- [16] Y.-H. Sung, W.-P. Liao, D.-W. Chen, C.-T. Wu, G.-J. Chang, J.-J. Wu, Room-temperature tailoring of vertical ZnO nanoarchitecture morphology for efficient hybrid polymer solar cells, *Adv. Funct. Mater.* 22 (2012) 3808–3814.
- [17] R. Zhu, C.-Y. Jiang, B. Liu, S. Ramakrishna, Highly efficient nanoporous TiO₂-polythiophene hybrid solar cells based on interfacial modification using a metal-free organic dye, *Adv. Mater.* 21 (2009) 994–1000.
- [18] J. Yu, T.-L. Shen, W.-H. Weng, Y.-C. Huang, C.-I. Huang, W.-F. Su, S.-P. Rwei, K.-C. Ho, L. Wang, Molecular design of interfacial modifiers for polymer-Inorganic hybrid solar cells, *Adv. Energy Mater.* 2 (2012) 245–252.
- [19] P. Ruankham, L. Macaraig, T. Sagawa, H. Nakazumi, S. Yoshikawa, Surface modification of ZnO nanorods with small organic molecular dyes for polymer-Inorganic hybrid solar cells, *J. Phys. Chem. C* 115 (2011) 23809–23816.
- [20] D.-W. Chen, T.-C. Wang, W.-P. Liao, J.-J. Wu, Synergistic effect of dual interfacial modifications with room temperature-grown epitaxial ZnO and adsorbed indoline dye for ZnO nanorod array/P3HT hybrid solar cell, *ACS Appl. Mater. Interfaces* 5 (2013) 8359–8365.
- [21] Y.-Z. Zheng, X. Tao, L.-X. Wang, H. Xu, Q. Hou, W.-L. Zhou, J.-F. Chen, Novel ZnO-based film with double light-scattering layers as photoelectrodes for enhanced efficiency in dye-sensitized solar cells, *Chem. Mater.* 22 (2010) 928–934.
- [22] Y.-Z. Zheng, J. Zhao, H. Zhang, J.-F. Chen, W. Zhou, X. Tao, Dual-functional ZnO nanorod aggregates as scattering layer in the photoanode for dye-sensitized solar cells, *Chem. Commun.* 47 (2011) 11519–11521.
- [23] F. Huang, D. Chen, X.L. Zhang, R.A. Caruso, Y.-B. Cheng, Dual-function scattering layer of submicrometer-sized mesoporous TiO₂ beads for high-efficiency dye sensitized solar cells, *Adv. Funct. Mater.* 20 (2010) 1301–1305.
- [24] L. Wang, F.Q. Tang, K. Ozawa, Z.G. Chen, A. Mukherj, Y.C. Zhu, J. Zou, H. Cheng, G. Q. Lu, A general dingle-source route for the preparation of hollow nanoporous metal oxide structures, *Angew. Chem. Int. Ed.* 121 (2009) 7048–7051.
- [25] W.C. Tsoi, D.T. James, J.S. Kim, P.G. Nicholson, C.E. Murphy, D.D.C. Bradley, J. Nelson, J.-S. Kim, The nature of in-plane skeleton raman modes of P3HT and their correlation to the degree of molecular order in P3HT: PCBM blend thin films, *J. Am. Chem. Soc.* 133 (2011) 9834–9843.
- [26] J.-J. Yun, J. Peet, N.-S. Cho, G.C. Bazan, S.J. Lee, M. Moskovits, Insight into the Raman shifts and optical absorption changes upon annealing polymer/fullerene solar cells, *Appl. Phys. Lett.* 92 (2008) 251912.
- [27] M.-S. Kim, B.-G. Kim, J. Kim, Effective variables to control the fill factor of organic photovoltaic cells, *ACS Appl. Mater. Inter.* 1 (2009) 1264–1269.
- [28] L. Zeng, C.W. Tang, S.H. Chen, Effects of active layer thickness and thermal annealing on polythiophene: fullerene bulk heterojunction photovoltaic devices, *Appl. Phys. Lett.* 97 (2010) 053305.
- [29] S. Lee, S. Nam, H. Kim, Y. Kim, Organic solar cells with submicron-thick polymer: fullerene bulk heterojunction films, *Appl. Phys. Lett.* 97 (2010) 103503.
- [30] H.J. Park, H. Kim, J.Y. Lee, T. Lee, L.J. Guo, Optimization of polymer photovoltaic cells with bulk heterojunction layers hundreds of nanometers thick: modifying the morphology and cathode interface, *Energy Environ. Sci.* 6 (2013) 2203–2210.
- [31] K. Yan, L. Zhang, J. Qiu, Y. Qiu, Z. Zhu, J. Wang, S. Yang, A quasi-quantum well sensitized solar cell with accelerated charge separation and collection, *J. Am. Chem. Soc.* 135 (2013) 9531–9539.
- [32] P. Ruankham, S. Yoshikawa, T. Sagawa, Effects of the morphology of nanostructured ZnO and interface modification on the device configuration and charge transport of ZnO/polymer hybrid solar cells, *Phys. Chem. Chem. Phys.* 15 (2013) 9516–9522.
- [33] P. Ruankham, S. Yoshikawa, T. Sagawa, Improved performance of hybrid ZnO/polymer solar cell via construction of hierarchical nanostructures and surface modification of ZnO, *Jpn. J. Appl. Phys.* (2014) 01AB14/1–4.
- [34] J.E. Kroeze, N. Hirata, L. Schmidt-Mende, C. Orizu, S.D. Ogier, K. Carr, M. Grätzel, J.R. Durrant, Parameters influencing charge separation in solid-state dye-sensitized solar cells using novel hole conductors, *Adv. Funct. Mater.* 16 (2006) 1832–1838.
- [35] N. Kudo, S. Honda, Y. Shimazaki, H. Ohkita, S. Ito, H. Benten, Improvement of charge injection efficiency in organic-inorganic hybrid solar cells by chemical modification of metal oxides with organic molecules, *Appl. Phys. Lett.* 90 (2007) 183513.